Effective interaction for ^{40}Ca(p,p') at $E_p = 318$ MeV

J. J. Kelly, P. Boberg, A. E. Feldman, B. S. Flanders,* M. A. Khandaker, S. D. Hyman,† and
H. Seifert‡
Department of Physics and Astronomy, University of Maryland, College Park, Maryland 20742

P. Karen, B. E. Norum, and P. Welch
Department of Physics, University of Virginia, Charlottesville, Virginia 22901

S. Nanda and A. Saha
Continuous Electron Beam Accelerator Facility, Newport News, Virginia 23606
(Received 30 May 1991)

Differential cross sections and analyzing powers have been measured for the excitation by 318 MeV protons of states of ^{40}Ca below 7.2 MeV. The data for those normal-parity excitations for which transition densities are available from electroexcitation measurements are analyzed in terms of medium modifications to the nucleon-nucleon interaction. We find that the empirical effective interaction previously fitted to ^{16}O(p,p') data at the same energy predicts ^{40}Ca(p,p') very well. Density-dependent modifications of the effective interaction fitted to data for ^{40}Ca or ^{16}O, either independently or simultaneously, are virtually identical. The density dependence of the empirical interaction is considerably stronger than that of interactions based upon nonrelativistic nuclear matter theory and persists to lower density. The most significant differences are that the empirical interaction has a stronger repulsive core and that absorption is enhanced at high density, contrary to expectations based upon Pauli blocking. We also find substantial suppression of the spin-orbit interaction at low density and enhancement at high density. Nevertheless, the independence of the effective interaction from the target supports the concept of local nuclear matter density. We also find that optical potentials based upon the empirical effective interaction are very similar to Schrödinger-equivalent potentials based upon a relativistic impulse approximation model, suggesting that the empirical density dependence is similar to the equivalent density dependence that arises from elimination of lower components from Dirac wave functions. Finally, the results are compared with global optical potentials from Dirac phenomenology.

I. INTRODUCTION

A variety of theoretical [1–3] and phenomenological [4,5] models of proton scattering for energies near 300 MeV have shown that the nonrelativistic effective interaction depends strongly upon density. These models rely upon the local density approximation (LDA) [6–9], which more aptly would be designated an hypothesis, that assumes that the effective interaction between an energetic projectile and a target nucleon depends upon the local density in the interaction region but not upon the specific target or transition. Theoretical calculations of the effective interaction are then made for infinite nuclear matter at several densities and applied to finite nuclei assuming that the nucleus resembles nuclear matter within the interaction region.

Three calculations of the effective interaction for 318-MeV protons are available. The Paris-Hamburg (PH) interaction [1] uses the Paris potential [10] to evaluate the correlated pair wave function in nuclear matter and then uses an extension [7] of the Siemens averaging procedure [11] to construct an effective interaction whose matrix elements for uncorrelated states are similar, on average, to those of correlated states. The Nakayama-Love (NL) interaction [2] uses the Bonn potential [12] and a pseudo-

potential prescription designed to reproduce on-shell matrix elements of the G matrix. Finally, the LR interaction due to Ray [3] uses a coupled-channels nucleon-isobar model [13] to evaluate the Watson optical potential [14] for energies above pion threshold. Unfortunately, the effective interactions that emerge from these models, which involve untested approximations, are significantly different and these differences affect scattering calculations appreciably [4]. These ambiguities are not confined to 300 MeV and complicate evaluation of the underlying local density hypothesis upon which the scattering calculations are based [15,16].

We have developed an empirical model of medium modifications to the effective interaction suitable for phenomenological analysis of scattering data [15]. The model is designed to reproduce the qualitative features of the nuclear matter calculations with a minimum number of free parameters. Comparisons between the parameters fitted to nuclear matter interactions and the parameters fitted to scattering data are more enlightening than a compilation of comparisons to individual angular distributions. Data are analyzed by varying the most important model parameters of the empirical effective interaction beginning from theoretical estimates. We include data for several states among several targets simultane-

ously to maximize sensitivity to density dependence and minimize vulnerability to peculiar characteristics of particular data sets.

Empirical effective interactions fitted to proton scattering from ^{16}O have been reported for 135, 180, 318, and 500 MeV [15,16,4,5]. For energies below 300 MeV we found that the density dependence of the empirical effective interaction appears to be somewhat less than theoretical estimates, but that modifications of the interaction are required even as the density approaches zero. This latter result conflicts with a strict interpretation of the LDA, which would require the interaction for low densities to reduce to the nucleon-nucleon t matrix in free space. We suggested that nonlocal effects in a finite nucleus might relax this restriction but still remain susceptible to a local description. Due to the finite extension of nucleon orbitals, it is reasonable to expect that medium modifications in the surface region are sensitive to the greater densities nearby and are thus stronger than predicted by the LDA. Similarly, medium modifications in the interior might be sensitive to the lower surface densities nearby and thus be weaker than predicted by the LDA.

For energies above 300 MeV [4,5] we found that empirical medium modifications are considerably stronger than predicted by nonrelativistic models. Most notably, absorption represented by the imaginary central interaction appears to be enhanced at high densities, whereas the Pauli blocking mechanism predicts damping. Contrary to the phase space Pauli blocking model of Clementel and Villi [17], which predicts that the damping coefficient is positive and is inversely proportional to energy, we found a small negative coefficient at 318 MeV and a larger negative coefficient at 500 MeV. We also found that the repulsive density-dependent contribution to the real central interaction is substantially stronger than theoretical estimates and is similar in strength at both 318 and 500 MeV, Finally, we found that the real spin-orbit interaction is damped at low density and enhanced at high density for energies above 300 MeV. Therefore, there appears to be a distinct qualitative change in the effective interaction that occurs near 300 MeV.

Previous analyses of the empirical effective interaction have fitted data for inelastic scattering only; predictions for elastic data were then used as an independent test of the self-consistency of the model. The primary motivation for fitting inelastic instead of elastic scattering data was that the availability of various transition densities localized near the surface or with significant interior contributions provides considerable differential sensitivity to the density dependence of the effective interaction, whereas elastic scattering is sensitive to an average over the entire nuclear volume and does not clearly differentiate between interior or surface contributions. Some additional sensitivity to the density dependence of the interaction is obtained by using distorted waves computed from optical potentials evaluated by folding the same effective interaction over the ground-state density, so that changes in the interior interaction affect both the distorted waves and the scattering potentials for transitions with significant interior contributions. The success

of this procedure requires inclusion of a rearrangement contribution, first derived by Cheon et al.[18], which effectively doubles the density dependence of the effective interaction for inelastic scattering relative to that for nuclear matter or for elastic scattering. However, some of the elastic scattering predictions made from interactions fitted to inelastic scattering indicate that the empirical density dependence may sometimes be too strong. Therefore, in this paper we extend the fitting procedures to include elastic scattering data.

At 180 MeV we found that both ^{16}O and ^{28}Si(p,p') could be fitted with a common interaction [16]. Similarly, at 500 MeV we fitted interactions to inelastic scattering data for ^{16}O and ^{40}Ca and showed that the data for both nuclei can be described very well with the same interaction [5]. In this paper we report additional data for ^{40}Ca(p,p') at 318 MeV and find that the interaction fitted to inelastic scattering from ^{16}O fits both elastic and inelastic scattering by ^{40}Ca very well. We also find that interactions fitted to ^{40}Ca elastic scattering data alone, or to ^{40}Ca inelastic scattering, or to both elastic and inelastic scattering simultaneously, are very similar to the interaction fitted to ^{16}O inelastic scattering. The density dependence of the real central component is somewhat smaller when the interaction is fitted to ^{40}Ca elastic scattering alone, but good agreement with the inelastic scattering data is still obtained for both nuclei. Therefore, convergence among the 318-MeV interactions for both ^{16}O and ^{40}Ca and for both elastic and inelastic scattering demonstrates that the effective interaction is very nearly independent of both target and state, in agreement with the local density hypothesis.

The experiment is described in Sec. II. The interaction model and fitting procedures, including the extension to elastic scattering, are presented in Sec. III. Fits to inelastic scattering and elastic scattering are presented in Secs. IV A and IV B, respectively. In Sec. IV C we show that the interaction fitted to ^{40}Ca data predicts elastic scattering for both ^{16}O and ^{208}Pb very well. The empirical effective interaction is compared with the IA2 version of the relativistic impulse approximation [19] and with Dirac phenomenology [20] in Sec. IV D. These comparisons are made using Schrödinger-equivalent optical potentials. Finally, our conclusions are summarized in Sec. V.

II. EXPERIMENT

The experiment was performed using 318-MeV protons provided by the Los Alamos Meson Physics Facility (LAMPF) to the High Resolution Spectrometer (HRS) during two periods separated by about a year. Standard equipment and techniques thoroughly documented elsewhere were employed [21,22]. The beam energies, as determined from known spectrometer properties, were typically 318.3$\pm$0.2 MeV during the first period and 317.8$\pm$0.3 MeV during the second. The beam polarizations were typically 0.7–0.8. Current monitors were calibrated by comparing measurements of pp elastic scattering made with CH$_2$ targets with phase shift calculations [23]. Two targets consisting of isotopically enriched

(> 99.9%) ^{40}Ca foils with areal thicknesses of 19.7 and 18.97 mg/cm^2 were used, with the bulk of the data collected on the second target during the second run. Cross sections for the two runs, with different targets, agreed to better than ±3%. Therefore, we estimate the normalization uncertainty to be about ±5%. Further details may be found in Ref. [24].

The ±1.0° HRS acceptance was subdivided into three equal bins of scattering angle. The spectra were analyzed using the ALLFIT line-shape fitting program [25]. A typical fitted spectrum, with a resolution of about 48 keV FWHM, is shown in Fig. 1. The 0_2^+ excited state, though weak, is clearly visible. The separations between peaks belonging to closely spaced clusters were constrained to known values [26].

Data were collected for angles between 3° and 39°, corresponding to momentum transfers between 0.3 and 2.8 fm^{-1}, for a total of 21 states below 7.2 MeV of excitation. Complete data tables on deposit with the Physics Auxiliary Publication Service (PAPS) [27]. In this paper we consider only the ground-state (0_1^+), 0_2^+ (3.352 MeV), 3_1^- (3.736 MeV), 2_1^+ (3.904 MeV), 5_1^- (4.492 MeV), 3_2^- (6.286 MeV), and 3_3^- (6.583 MeV) states for which transition charge densities are available from independent electroexcitation measurements [28–30].

III. EMPIRICAL EFFECTIVE INTERACTION

A. Model

Our implementation of the folding model and parametrization of the effective interaction have been presented in considerable detail within a series of previous papers reporting empirical effective interactions for $135 \leq E_p \leq 500$ MeV [4,5,15,16]. Therefore, only a few brief comments are needed here. Assuming that $\rho_n = \rho_p$ for self-conjugate targets and neglecting small current and spin densities for normal-parity excitations, electron scattering measurements suffice to determine the nuclear
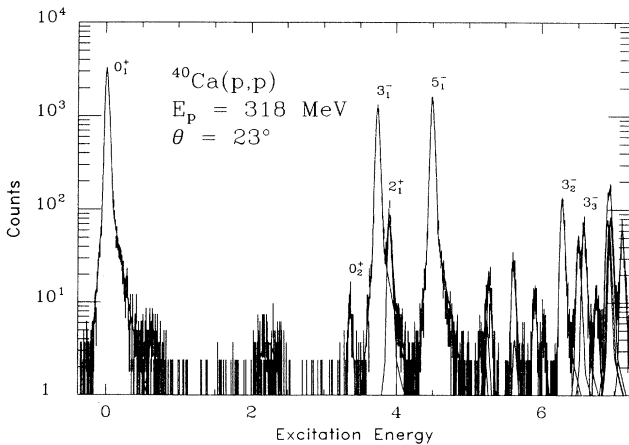

FIG. 1. Typical fitted spectrum for ^{40}Ca(p,p') at 318 MeV plotted on a semilogarithmic scale. Peaks corresponding to the states analyzed in this paper are labeled with multipolarity J_n^π. Note that the 0_2^+ peak, though weak, is clearly visible.

structure information required to study the effective interaction. Optical potentials are produced by folding an effective interaction with the ground-state density obtained by correcting the charge density of Ref. [28] for the proton form factor and assuming $\rho_n = \rho_p$. Similarly, transition densities for the 2_1^+, 3_1^-, 3_2^-, 3_3^-, and 5_1^- states of ^{40}Ca were obtained by unfolding the proton form factor from the transition charge densities fitted by Miskimen to electroexcitation data [29]. Finally, the 0_2^+ density was obtained from the electron scattering results of Harihar *et al.*[30].

The spherical optical potential can be written in the form

$$U(r) = U^Z(r) + U^C(r) + U^{LS}(r)\mathbf{L}\cdot\boldsymbol{\sigma} , \qquad (1)$$

where

$$U^{LS}(r) = \frac{1}{r}\frac{\partial F^{LS}}{\partial r} . \qquad (2)$$

Similarly, normal-parity isoscalar transitions are excited by scattering potentials of the form

$$U(\mathbf{r}) = U^Z(\mathbf{r}) + U^C(\mathbf{r}) + \nabla F^{LS}(\mathbf{r})\otimes\frac{1}{i}\nabla\cdot\boldsymbol{\sigma} , \qquad (3)$$

where U^Z is the potential obtained by folding the Coulomb interaction with either the ground-state or transition charge density. The central and spin-orbit potentials U^C and F^{LS} are obtained by folding the matter transition density ρ_J with central and spin-orbit components of the effective interaction t^C and τ^{LS} according to

$$U_J^C(r) = \frac{2}{\pi}\int dq\, q^2 j_J(qr)\eta t^C(q,\rho_G(r))\rho_J(q) , \qquad (4a)$$

$$F_J^{LS}(r) = \frac{2}{\pi}\int dq\, q^2 j_J(qr)\eta \tau^{LS}(q,\rho_G(r))\rho_J(q) , \qquad (4b)$$

where ρ_G is the local ground-state matter density. The Jacobian between nucleon-nucleon and nucleon-nucleus frames is denoted by η [31,32].

For simplicity, the effective interaction is evaluated for the local density at the site of the projectile; the differences obtained for alternative choices of local density, such as the position of the struck nucleon or the two-body center of mass, are much smaller than the ambiguities due to the choice of interaction [9]. The effective interaction for elastic scattering should be similar to the G matrix for nuclear matter, whereas the density dependence of the effective interaction t' appropriate to inelastic scattering is stronger than the elastic $t(q,\rho)$ produced by nuclear matter theories due to a rearrangement factor of the form [18]

$$t' = (1 + \rho\, \partial/\partial\rho)t . \qquad (5)$$

We have found at several energies between 100 and 500 MeV that this factor is essential to a consistent description of elastic and inelastic scattering with either theoretical or empirical effective interactions. Therefore, this factor is employed in the present analysis also.

Sensitivity to the density dependence of the effective interaction is greatly enhanced by the availability of several

states with a variety of transition densities, some concentrated at the nuclear surface and others with significant interior contributions. The transition densities deduced from electroexcitation measurements [29,30] for the six inelastic transitions selected for study in ^{40}Ca are displayed in Fig. 2. The 2_1^+, 3_1^-, and 5_1^- transitions are clearly most sensitive to the low-density properties of the effective interaction, whereas the 0_2^+, 3_2^-, and 3_3^- transitions offer sensitivity to the interaction at saturation density.

We have shown that the density dependencies for each of the theoretical interactions available at 318 MeV can be parametrized in a form suitable for phenomenological analysis of nucleon-nucleus scattering data. The relevant terms of the effective interaction are described by the parametrization [4]

$$\mathrm{Re}t^C(q,\kappa) = S_1 \mathrm{Re}t_f^C(q) + b_1 \kappa^3 [1 + (q/\mu_1)^2]^{-1} , \tag{6a}$$

$$\mathrm{Im}t^C(q,\kappa) = [S_2 - d_2\kappa^2]\mathrm{Im}t_f^C(q) , \tag{6b}$$

$$\mathrm{Re}\tau^{LS}(q,\kappa) = S_3 \mathrm{Re}\tau_f^{LS}(q) + b_3 \kappa^3 [1 + (q/\mu_3)^2]^{-2} , \tag{6c}$$

where $\kappa = (k_F/1.33)$ represents the local Fermi momentum relative to saturation. The scale factors S_1, S_2, and S_3 permit modification of the "free" interactions t_f^C and τ_f^{LS} at low densities; these factors are constrained to unity for theoretical interactions and should be near unity for phenomenological analyses if the strict interpretation of

the local density approximation is valid. The Yukawa-like terms in the real central and spin-orbit interactions represent short-range repulsive interactions. The damping factor applied to the imaginary central interaction was originally intended to represent the effect of Pauli blocking. However, although the theoretical interactions predict positive values of d_2 consistent with the Pauli-blocking interpretation, fits to the data for ^{16}O(p,p') and ^{40}Ca(p,p') at 500 MeV and for ^{16}O(p,p') at 318 MeV produce negative values for d_2. Equivalent fits were obtained constraining d_2 to the positive value predicted by the LR interaction while varying the amplitude of a Yukawa contribution to the imaginary central interaction; hence, these analyses suggest that either a new absorptive mechanism sufficiently strong to mask the Pauli blocking effect is present or that the phenomenological "damping factor" deviates strongly from theoretical predictions for energies above 300 MeV. However, because the three predictions for d_2 differ substantially, it is simpler to vary d_2 without additional Yukawa contributions than it is to constrain d_2 to a value of unknown reliability and allow the error in d_2 to affect the fitted value of b_2.

Therefore, fits to data were made using six free parameters $\{S_1, b_1, S_2, d_2, S_3, \text{and } b_3\}$. The strength and density dependence of the imaginary spin-orbit interaction are too small to obtain stable fits of these components; therefore, except where explicitly indicated otherwise, the
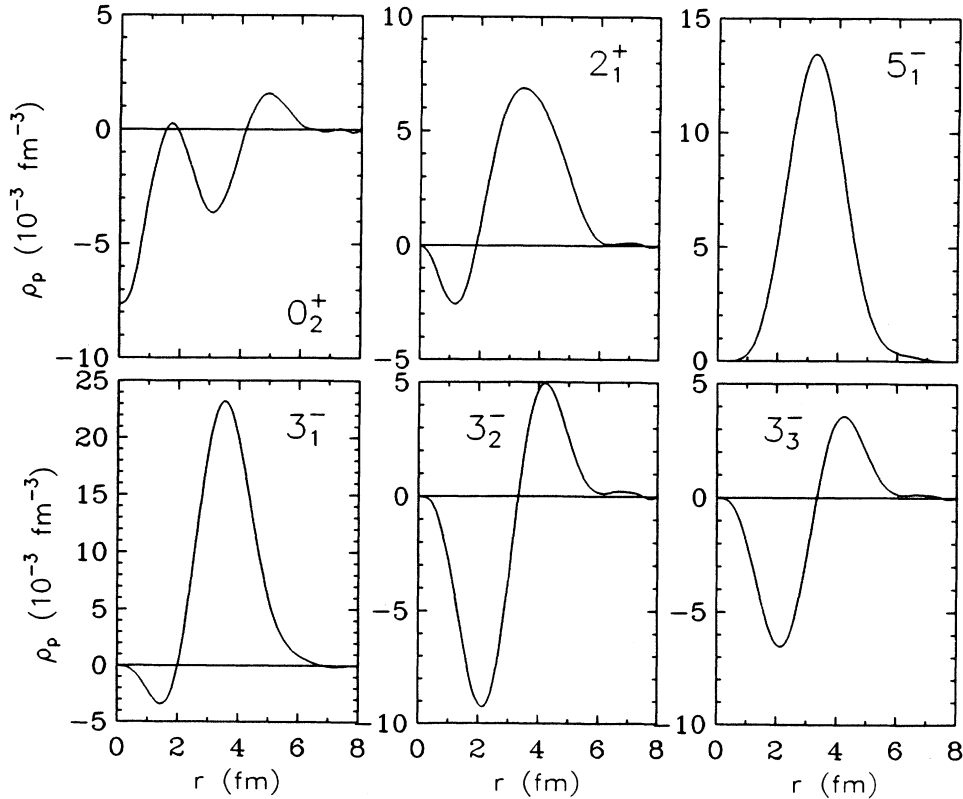

FIG. 2. Point-proton transition densities for states of ^{40}Ca. Notice that the 0_2^+, 3_2^-, and 3_3^- densities include considerable interior strength and are therefore sensitive to the interaction near saturation density.

parameters of $\mathrm{Im}\tau^{LS}$ were constrained to the parametrization of the LR interaction given in Ref. [4]. The mass parameters $\mu_1 = 2.0 \text{ fm}^{-1}$ and $\mu_3 = 6.0 \text{ fm}^{-1}$ were chosen to give a good description the LR interaction at 320 MeV. We have chosen to use the Franey-Love (FL) t matrix to describe the free interaction [32].

B. Fitting procedures

The requirement that both the inelastic scattering potentials and the distorted waves be generated from the same effective interaction necessitates a self-consistency cycle. Given an initial model of the effective interaction, distorted waves and overlap integrals are computed for each transition analyzed. The parameters of the effective interaction are then adjusted to fit the data without variation of the distorted waves. The fitted parameters are then used to compute new optical potentials, distorted waves, and overlap integrals for the next fitting iteration. To improve the stability of the procedure, the distorted waves for a given iteration are based upon the average of the parameters from the preceding two iterations.

Previous analyses of the empirical effective interaction have fitted only inelastic scattering data. This limitation was partly motivated by practical considerations of computation time and partly to preserve an independent means of testing the internal consistency of the model. The accuracy with which an interaction fitted to inelastic scattering data alone is able to predict elastic scattering data which were not included in the analysis constitutes a stringent test of self-consistency. We indeed found that interactions fitted to inelastic scattering data for 135-, 180-, 318-, and 500-MeV protons did predict elastic scattering relatively accurately. However, there were indications that the density dependence fitted to inelastic scattering data may sometimes be stronger than needed for an optimal fit of elastic scattering data. Therefore, it is of interest to extend the fitting procedures to include elastic scattering.

We represent the effective interaction $t = \sum_n a_n t_n$ as a linear expansion where the t_n represent basis functions and the a_n the parameters of the model, which in this case include the free parameters $\{S_i, b_i, d_i\}$ and the fixed parameters. The optical potential $U = \sum_n a_n U_n$ and the scattering potentials $\Delta U_n = \sum_n a_n \Delta U_n$ for each transition can then be expressed as similar expansions based upon the same parameters a_n and N basis functions obtained from folding each interaction term t_n with the appropriate nuclear density or transition density. In the distorted wave approximation, the nucleon-nucleus scattering amplitude for inelastic scattering is then an expansion $T = \sum_n a_n T_n$ where each basis function is obtained from the overlap of the scattering potential with the current set of distorted waves χ. So that both elastic and inelastic scattering may be computed from similar formulas, it is convenient to define an auxiliary set of coefficients $\{c_n, n = 0, N\}$ where

$$c_0 = 0 \quad \text{(inelastic)}$$
$$= 1 \quad \text{(elastic)} \; ,$$

$$c_n = a_n \quad \text{(inelastic, } n > 0)$$
$$= \delta a_n \quad \text{(elastic, } n > 0) \; ,$$

and where the coefficients δa_n are the differences between the current parameters and those that were used to compute the distorted waves. The distorted-wave approximation to the scattering amplitudes for either elastic or inelastic scattering can then be expressed as expansions of the form

$$T = \sum_{n=0}^{N} c_n T_n \; , \tag{7}$$

where

$$T_0(\theta) = -\frac{2\pi}{\mu} f(\theta) \quad \text{(elastic)} \; , \tag{8a}$$

$$T_n(\theta) = \langle \chi_f | U_n | \chi_i \rangle \quad \text{(elastic, } n > 0) \; , \tag{8b}$$

$$T_n(\theta) = \langle \chi_f | \Delta U_n | \chi_i \rangle \quad \text{(inelastic)} \; , \tag{8c}$$

and where $f(\theta)$ is the elastic scattering amplitude deduced from the phase shifts for the present set of distorted waves. The factor $(-2\pi/\mu)$ is applied to the conventional $f(\theta)$ so that both elastic and inelastic amplitudes are normalized consistently.

The observables are most efficiently evaluated as contractions of the quadratic forms

$$X_{\alpha\beta}^{nn'}(\theta) = \mathrm{Tr}[T^n(\theta)\sigma_\alpha T^{n'}(\theta)^* \sigma_\beta] \tag{9}$$

which are independent of the fitting parameters and hence may be computed and stored for each state at the beginning of each cycle. We then find that the observables may be expressed as

$$\frac{d\sigma}{d\Omega} = \frac{\mu_i \mu_f}{(2\pi)^2} \frac{k_f}{k_i} \frac{I_0(\theta)}{(2j_i + 1)} \; , \tag{10a}$$

$$I_0(\theta) = \frac{1}{2} \sum_{nn'} c_n X_{00}^{nn'}(\theta) c_{n'}^* \; , \tag{10b}$$

$$I_0 D_{\alpha\beta} = \frac{1}{2} \sum_{nn'} c_n X_{\alpha\beta}^{nn'}(\theta) c_{n'}^* \; , \tag{10c}$$

where j_i is the target spin and where μ_i (μ_f) and k_i (k_f) are reduced energies and projectile wave numbers in the initial (final) channel.

The analyzing power $A_y = D_{y0}$ and induced polarization $P = D_{0y}$ are special elements of the depolarization matrix $D_{\alpha\beta}$ where α and β denote the orientation of projectile polarization vectors in the initial and final channels, respectively [33]. For inelastic scattering, these orientations are usually referred to helicity bases $(\hat{\mathbf{S}}, \hat{\mathbf{N}}, \hat{\mathbf{L}})$ where $\hat{\mathbf{L}}$ is along the momentum of the projectile in the initial channel and the detected nucleon in the final channel and where $\hat{\mathbf{N}}$ is normal to the scattering plane. For elastic scattering, it is common to express the in-plane polarization observable as the spin rotation function $\mathrm{SRF} = D_{zx}$ where the $(\hat{\mathbf{x}}, \hat{\mathbf{y}}, \hat{\mathbf{z}})$ basis is referred to laboratory coordinates with $\hat{\mathbf{z}}$ along the beam direction and $\hat{\mathbf{y}}$ normal to the scattering plane; this system coincides with the projectile helicity frame in the initial channel.

This linear expansion analysis establishes the foundation of an efficient search algorithm that is implemented in the computer program LEA [34]. The basis potentials U_n or ΔU_n for each state are independent of the interaction coefficients a_n and hence may be computed once and stored. Given a good initial guess for the parameters $\{a_n\}$, distorted waves χ and scattering amplitudes T_n for each transition can then be calculated and stored. It is now a simple matter to minimize χ^2 with respect to the coefficients of the quadratic forms in Eq. (10); we use an algorithm based upon the CURFIT routine of Bevington [35]. New distorted waves and scattering amplitudes are then computed based upon the parameters of the preceding iteration and a new optimization is performed. This self-consistency cycle continues until both χ^2 and the parameters converge, usually in less than 10 iterations.

For the purpose of assigning similar weights to the data for all states and observables throughout the fitted range of momentum transfer, we fold additional uncertainties of $\pm5\%$ into cross-section data and ±0.05 into data for spin observables. The fits are restricted to momentum transfers $q \leq 2.7$ fm^{-1}, because both the electromagnetic form factors and the validity of the reaction model tend to be limited to about twice the Fermi momentum. Of course, data for the entire measured range are plotted with their original error bars.

IV. RESULTS

A. Comparison between interactions for ^{16}O and ^{40}Ca

Inelastic scattering calculations based upon the t matrix of Franey and Love (FL), the effective interaction of Ray (LR), and the empirical effective interaction (EI-3) are compared with the data in Figs. 3–5. We find that the impulse approximation, represented by the FL interaction, produces angular distributions whose structures are generally too oscillatory and analyzing powers that are systematically more positive than the data, particularly at small momentum transfers. The FL cross sections fall well below the high-q data for several states, especially the 5_1^- state. The density dependence of the LR interaction produces considerable improvement between theory and experiment, particularly for the 5_1^- cross section calculation, but still does not adequately suppress the low-q analyzing power or the oscillation of the 2_1^+ cross section. We also find that the elastic cross section is too small at low momentum transfers. Similar results were found for ^{16}O at 318 MeV also [4].

Notice that the cross-section angular distributions for the second and third 3^- states are distinctly different from the first, indicating sensitivity to the differences between these transition densities. The strong interior lobes
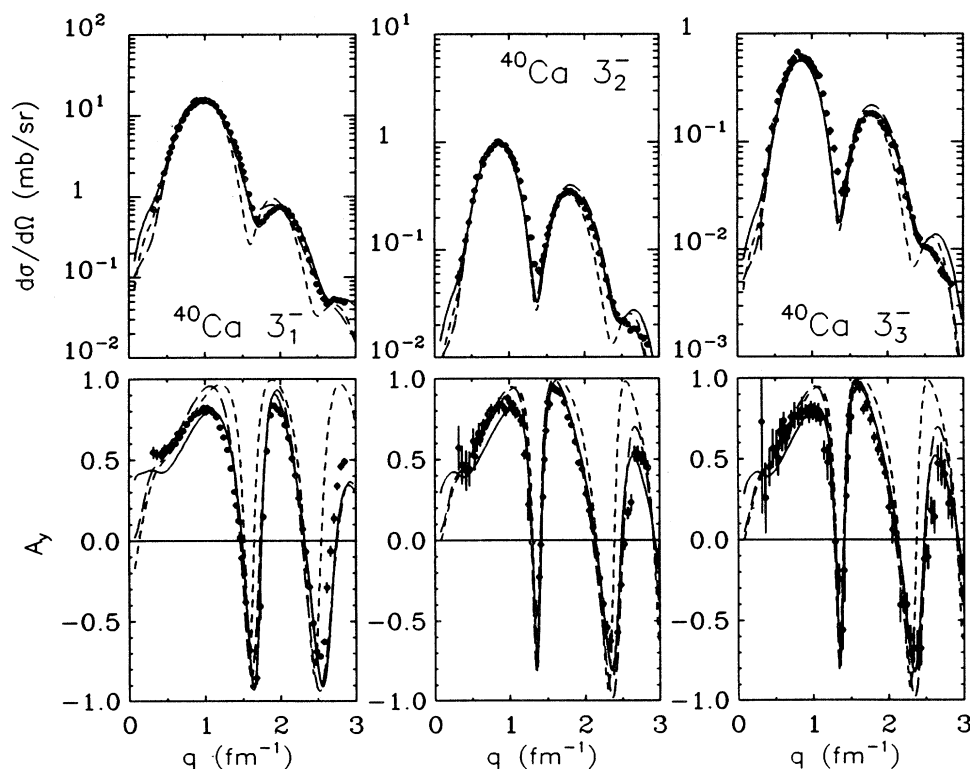

FIG. 3. Calculations for the 3_1^-, 3_2^-, and 3_3^- states of ^{40}Ca based upon the FL and LR interactions, shown as short-dashed and long-dashed curves, are compared with fits to the inelastic scattering data, shown by the solid lines. Differences between fits made using inelastic data for ^{16}O and ^{40}Ca, either individually or simultaneously, are indistinguishable on these figures.

TABLE I. Comparison between theoretical and empirical models of the effective interaction for 318-MeV nucleons. Parentheses indicate a constrained parameter. The notations "in" or "el" indicate fits to inelastic or elastic data. The ranges were chosen as $\mu_1 = 2.0$ fm^{-1} and $\mu_3 = 6.0$ fm^{-1}. The units are MeV-fm^3 for b_1 and MeV-fm^5 for b_3.

Model	S_1	b_1	S_2	d_2	S_3	b_3	Data set(s)
PH	(1.0)	60.1	(1.0)	0.057	(1.0)	1.17	
NL	(1.0)	35.2	(1.0)	0.219	(1.0)	0.40	
LR	(1.0)	61.2	(1.0)	0.267	(1.0)	1.74	
EI-1	1.068	144.7	1.021	−0.067	0.833	7.14	^{16}O in
EI-2	1.039	140.0	1.003	−0.014	0.776	5.25	^{40}Ca in
EI-3	1.070	142.2	1.001	−0.042	0.781	5.88	^{16}O, ^{40}Ca in
EI-4e	1.065	90.6	0.927	−0.025	0.849	3.28	^{40}Ca el
EI-4	1.122	120.4	1.010	−0.029	0.794	5.45	^{40}Ca el+in
EI-5	1.136	131.9	1.031	−0.059	0.810	6.07	^{16}O, ^{40}Ca el+in

of the 3_2^- and 3_3^- transition densities, displayed in Fig. 2, enhance the ratios between the second and first peaks of the cross section for these states. These enhancements demonstrate that there is enough penetrability at this energy to sample the effective interaction near saturation density.

Three fits of the empirical effective interaction to inelastic scattering data for 318-MeV protons are compared in Table I. Interaction EI-1, reported in Ref. [4], was fitted to inelastic scattering data for five states of ^{16}O simultaneously. Interaction EI-2 was fitted to the present inelastic data for these six states of ^{40}Ca. Interaction EI-3 was fitted to both data sets simultaneously, comprising a total of 22 angular distributions among 11 states. All three analyses began with initial parameters taken from the LR interaction and consisted of self-consistency cycles in which the distorting potentials for each iteration were constructed from the average of the fitted parameters from the previous two iterations. It is remarkable that despite the substantial difference between the initial
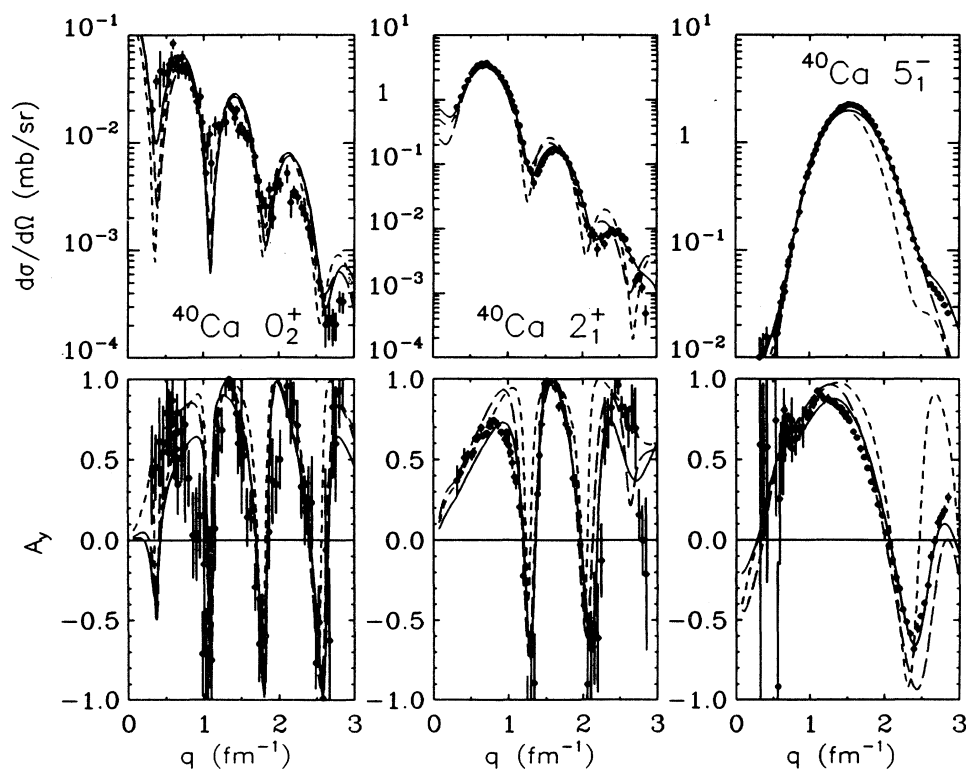

FIG. 4. Calculations for the 0_2^+, 2_1^+, and 5_1^- states of ^{40}Ca based upon the FL and LR interactions, shown as short-dashed and long-dashed curves, are compared with fits to the inelastic scattering data, shown by the solid lines. Differences between fits made using inelastic data for ^{16}O and ^{40}Ca, either individually or simultaneously, are indistinguishable on these figures.

and final parameter sets, and fluctuations early in the search paths, independent fits to data for different nuclei converge upon almost identical effective interactions. Most of the parameters fitted to the combined data set lie between the fits made to the two independent data sets. The differences between these three interactions, which produce virtually indistinguishable scattering calculations, are inconsequential.

The differences between LR and EI calculations for ^{40}Ca are generally smaller than previously found for ^{16}O because, with less absorption, scattering from ^{16}O is more sensitive to the nuclear interior. Nevertheless, the same interaction describes the data for both nuclei very well, supporting the hypothesis that the effective interaction depends primarily upon local density rather than the detailed structure of a specific target. For ^{40}Ca we find that the 2_1^+ cross section is improved significantly and that the large positive analyzing powers predicted for all states by both the FL and LR interactions near $q = 1$ fm^{-1} are reduced so that better agreement with the data is achieved.

Calculations for elastic scattering by ^{40}Ca predicted by the interaction fitted to inelastic scattering from ^{16}O are compared in Fig. 5 with our cross section and analyzing power data and with the measurements of the spin rotation function (SRF) reported in Ref. [36]. Calculations based upon the density-independent FL interaction and

the density-dependent LR interaction are also shown for comparison. Although the LR interaction achieves a significant improvement over the impulse approximation, its low-q analyzing power predictions remain too large. We also notice that the LR interaction predicts low-q cross sections significantly below the elastic data for ^{40}Ca and that this deficiency is even larger for ^{16}O elastic scattering [4]. The enhanced density dependence of the Ret^C and Reτ^{LS} components of the empirical interaction is needed to reproduce the detailed oscillatory structure of both the analyzing power and spin rotation data using a Schrödinger representation of the reaction. Reduction of the LR damping parameter d_2 restores the low-q elastic cross-section predictions to agreement with the data.

On the other hand, analyzing powers for $q < 1$ fm^{-1} now fall systematically below the data for inelastic scattering. This tendency is also seen for ^{16}O even though the low-q data are not as complete as these [4]. Therefore, it is likely that a common defect remains in the reaction mechanism rather than in the nuclear structure. One possibility is that the Cheon rearrangement model is not sufficiently accurate at this energy. For ^{16}O we found that the interaction fitted to inelastic scattering data produces changes in the elastic calculations that, although qualitatively correct, appear to be too strong; however, similar calculations for ^{40}Ca are more accurate.
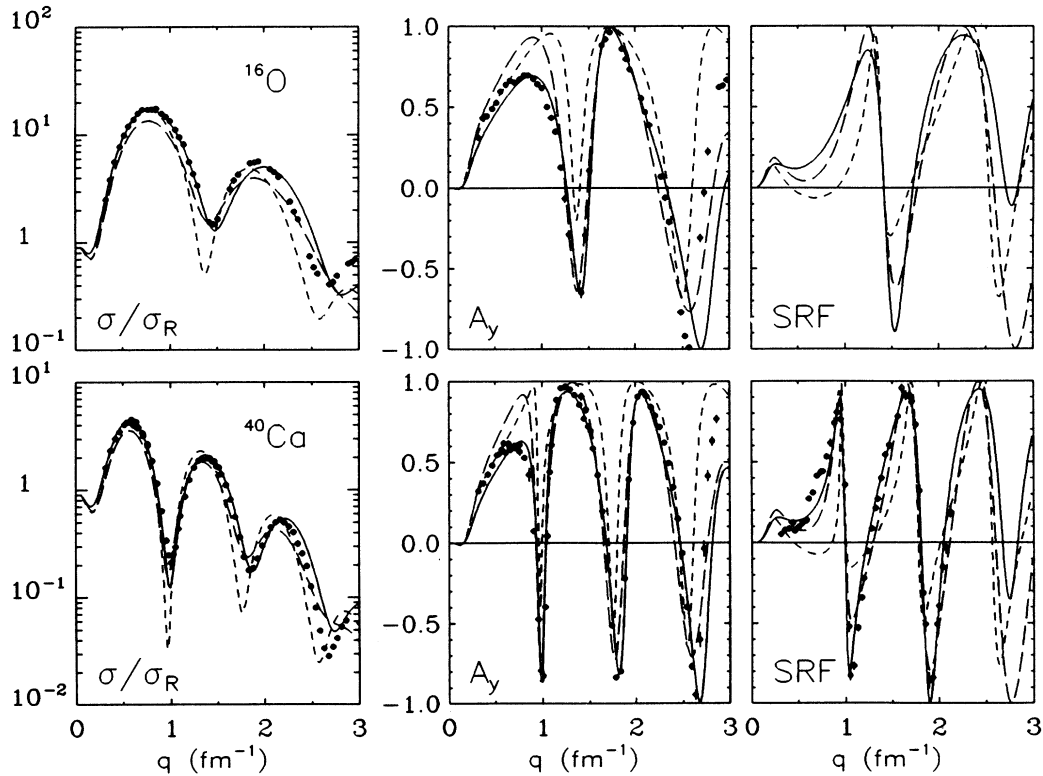

FIG. 5. Calculations for elastic scattering by ^{16}O (top row) and ^{40}Ca (bottom row) based upon the FL and LR interactions, shown as short-dashed and long-dashed curves, are compared with fits to the inelastic scattering data, shown by the solid lines. Differences between fits made using inelastic data for ^{16}O and ^{40}Ca, either individually or simultaneously, are indistinguishable on these figures. The elastic cross sections are shown as ratios to the Rutherford cross section (σ_R) to enhance detail.
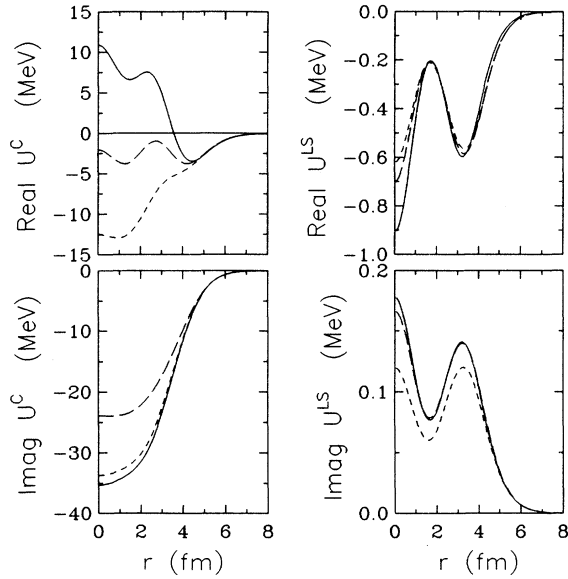
FIG. 6. Optical potentials for ^{40}Ca elastic scattering at 318 MeV calculated from the FL, LR, and EI-3 interactions are shown by short-dashed, long-dashed, and solid lines respectively.

Alternatively, the density dependence of the imaginary spin-orbit interaction is too small to fit to the data but may not be accurately predicted by the LR model. Finally, the empirical interaction requires a model of the free interaction as input, yet finds it necessary to scale the spin-orbit interaction for zero density. Perhaps the remaining systematic error in the effective interaction is due to q-dependent modifications of the low-density interaction that are not adequately represented by scaling.

The density dependence of the empirical interaction is illustrated in Fig. 6 by comparing optical potentials for ^{40}Ca for the free interaction (short dashes), the LR theoretical effective interaction (long dashes), and the

EI-3 empirical effective interaction (solid). The repulsive contribution to $\mathrm{Re} t^C$ is about twice as strong for the empirical interaction as it is for the LR interaction, resulting in a positive central depth of about 11 MeV for $\mathrm{Re} U^C$ instead of about -2 for the LR interaction or -12 for the FL t matrix. For $\mathrm{Im} U^C$, on the other hand, Pauli blocking in the LR interaction damps the absorptive potential in the interior, whereas absorption in the empirical interaction is slightly enhanced with respect to the t matrix. This result can be interpreted either as a change in the blocking mechanism or as a new contribution to the absorptive interaction that is present for energies above 300 MeV [4,5].

The parameters of the empirical interactions are compared in Table I with the LR theory and, for ease of comparison, with simplified parametrizations of the PH and NL interactions using the same choice of ranges; more accurate but more complicated parametrizations may be found in Ref. [4]. Comparing the parameters of the empirical interaction with those of the LR theory, we find that it is primarily the decrease in d_2 that improves the low-q elastic cross section. The corresponding parameter of the PH model is smaller and hence, as noted in Ref. [4], this interaction gives more accurate low-q cross sections than either the LR or NL interactions. Similarly, reduction of S_3 is primarily responsible for reducing the low-q analyzing power calculations whereas increasing b_1 yields the improvement in high-q cross section. Although the precise values of the fitted parameters are affected by correlations among the parameters and by the choice of ranges, these essential characteristics of the empirical effective interaction remain unambiguous. On the other hand, changes in the S_1, S_2, and b_3 parameters are used by the fit primarily for fine tuning; in fact, little is lost by constraining both S_1 and S_2 to unity. We also find that b_3 is not strongly determined by these data. Nevertheless, it is encouraging that all three fits to the inelastic data yield essentially the same parameters. Evidently, these data are of sufficient quality to determine the interaction uniquely.
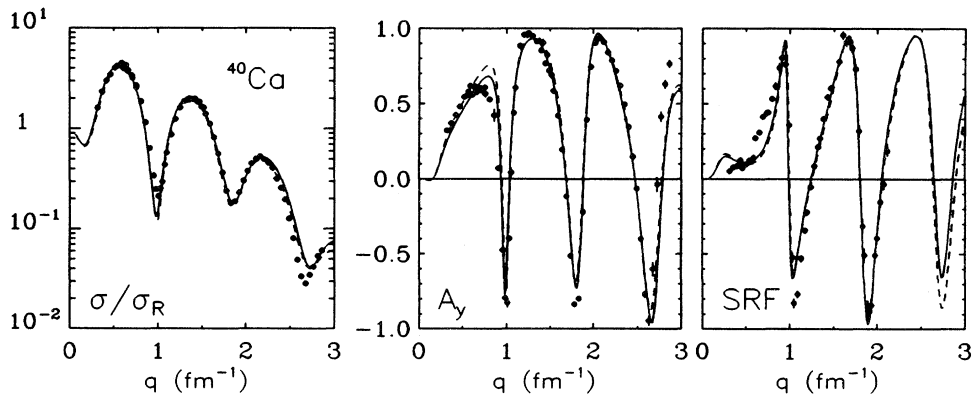

FIG. 7. Calculations for elastic scattering based upon interactions fitted to elastic scattering alone or in conjunction with inelastic scattering from ^{40}Ca are shown as dashed or solid curves, respectively.

B. Fits to elastic scattering

To test the self-consistency relationship between elastic and inelastic scattering, we performed a fit (EI-4e) to the elastic scattering data for ^{40}Ca alone, including our cross section and analyzing power measurements and the spin rotation data of Ref. [36]. We also performed a fit (EI-4) to the elastic and inelastic scattering data for ^{40}Ca simultaneously. These fits were initiated using the EI-3 parameters previously fit to inelastic scattering for ^{16}O and ^{40}Ca. The resulting parameters are also listed in Table I and the fits to the data are compared in Figs. 7–9. The primary difference between these interactions is found in the b_1 parameter; elastic scattering favors a smaller value for b_1 than inelastic scattering so that the simultaneous fit of elastic and inelastic scattering arrives at an intermediate value. The effects of these differences in b_1 upon the observables and upon χ^2 are quite small. Reduction of b_1 tends to yield slightly smaller cross sections for large momentum transfers and slightly larger analyzing powers for small momentum transfers. The former effect improves the agreement for elastic scattering but worsens the agreement for several inelastic transitions. The latter effect tends to improve the agreement with data below the first peak of the analyzing power but gives predictions that are somewhat too large immediately before the first sharp oscillation of the analyzing power.

The optical potentials that emerge from fits including elastic scattering data for ^{40}Ca are compared in Fig. 10 to those from fits to inelastic scattering alone. We find that the differences between the various interactions are very small for the spin-orbit and the imaginary central potentials, but that the differences between the b_1 parameters for these interactions produce significant variations of the real central potential in the interior. The strong b_1 in either EI-1 or EI-3 leads to the largest positive potential in the interior, whereas the smaller repulsion in the EI-4e fit to elastic scattering produces a shallower potential in the interior. Because the fits to the elastic data are not that different, we conclude that there must be a significant uncertainty in the value of b_1. Nevertheless, it is clear that b_1 is substantially larger than predicted by the LR interaction. We will also find in Sec. IV C that the EI-4 result, fitted to both elastic and inelastic scattering, is almost identical to the prediction of the relativistic IA2 model. Therefore, we favor the result with an intermediate value for b_1 that compromises between the tendency of inelastic data to favor larger b_1 and elastic data to favor smaller b_1.

Finally, we performed a fit to the entire data set, ^{16}O and ^{40}Ca elastic and inelastic, and obtained the result labeled EI-5 in Table I. The properties of this interaction are intermediate between EI-3 and EI-4, as expected.

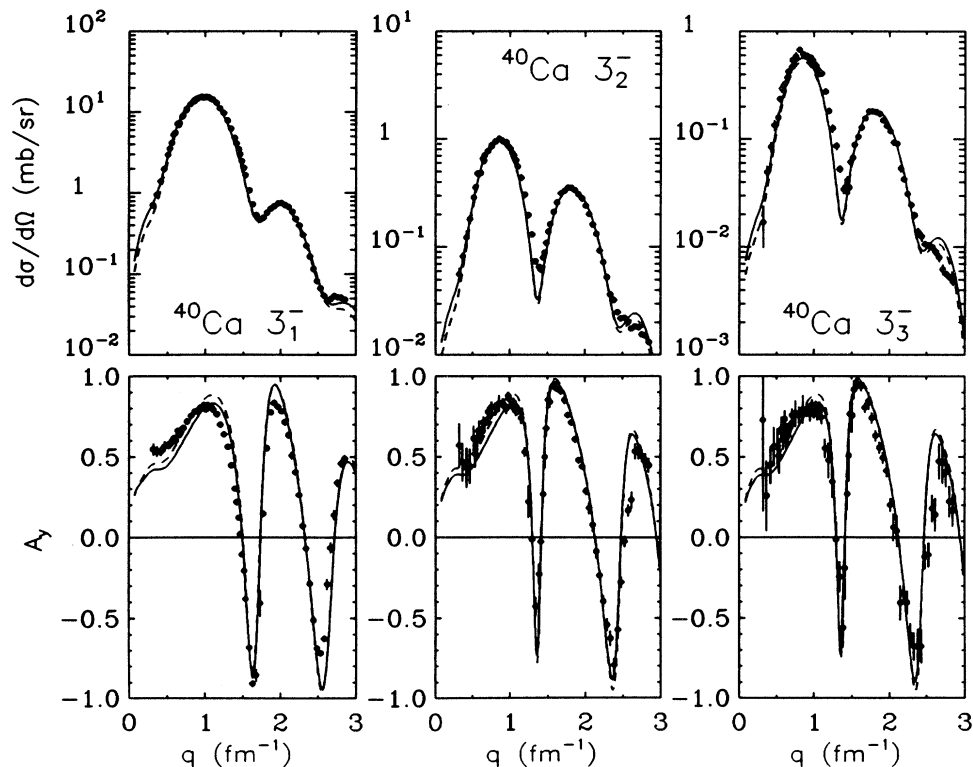The small but systematic discrepancies that remain in low-q analyzing power calculations and the sensitivity of

FIG. 8. Calculations for the 3_1^-, 3_2^-, and 3_3^- states of ^{40}Ca based upon interactions fitted to elastic scattering alone or in conjunction with inelastic scattering from ^{40}Ca are shown as dashed or solid curves, respectively. Notice that the fit made to elastic scattering alone provides almost as good a description of the inelastic data as fits to the inelastic data themselves.
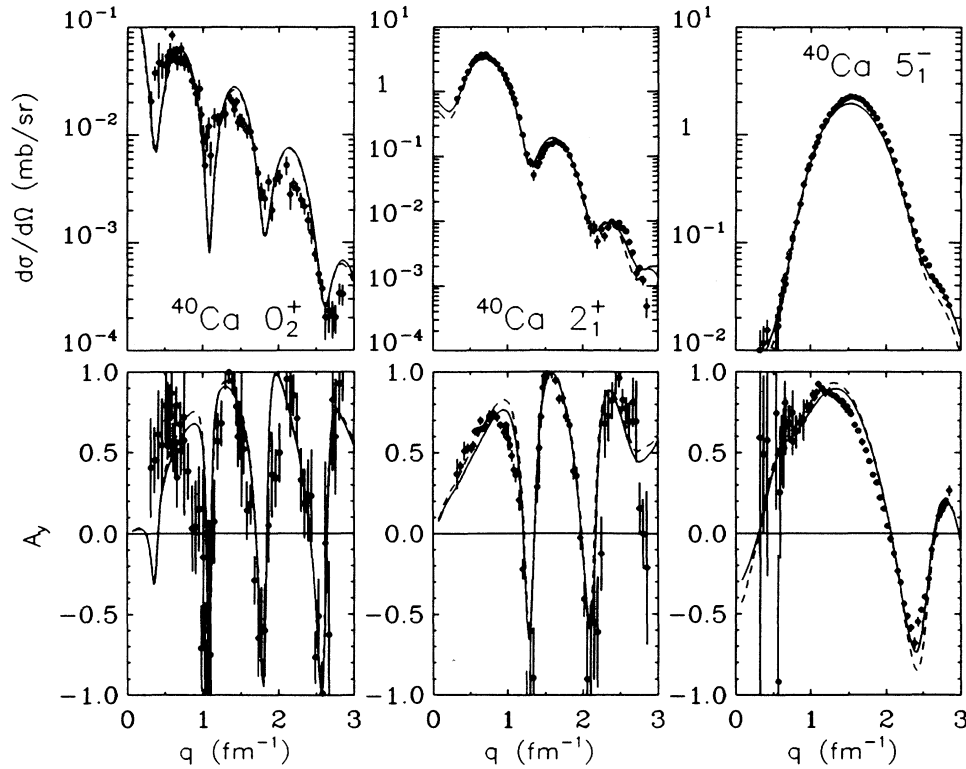
FIG. 9. Calculations for the 0_2^+, 2_1^+, and 5_1^- states of ^{40}Ca based upon interactions fitted to elastic scattering alone or in conjunction with inelastic scattering from ^{40}Ca are shown as dashed or solid curves, respectively. Notice that the fit made to elastic scattering alone provides almost as good a description of the inelastic data as fits to the inelastic data themselves.
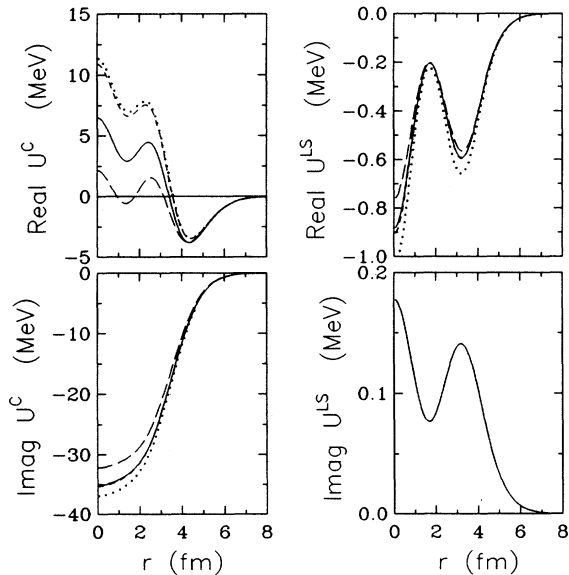

FIG. 10. Optical potentials for ^{40}Ca elastic scattering at 318 MeV calculated from the EI-3, EI-4e, and EI-4 interactions are shown by short-dashed, long-dashed, and solid lines, respectively. We also show the potentials calculated from the EI-1 interaction, fitted to inelastic scattering from ^{16}O without any ^{40}Ca data, by the dotted lines.

A_y for low-q to b_1 suggest that modification of the momentum transfer dependence of the real central interaction might improve the fit to the data. We performed fits to the elastic and inelastic scattering data for ^{40}Ca, both independently and simultaneously, varying μ_1 in steps of 0.5 fm^{-1} between 1.0 and 2.5 fm^{-1}. We find that slightly better fits to the elastic data can be obtained using smaller values of μ_1 and larger values of b_1, such that the real central interaction is reduced for q near 3 fm^{-1} but is preserved for q near 1 fm^{-1}. The remaining five parameters are almost independent of the choice of μ_1. Fits to the inelastic data, on the other hand, prefer somewhat larger values of μ_1. Thus, when fitting elastic and inelastic data simultaneously, we find that the original value of $\mu_1 = 2.0$ fm^{-1} corresponds to a shallow χ^2 minimum and that variation of μ_1 does not systematically improve the fit to the analyzing power data. We also attempted to fit the strength of the imaginary spin-orbit interaction, which was constrained in earlier analyses, but again find that the data are insensitive to even relatively large changes in this component of the interaction. We did not attempt to modify the low density interaction t_f beyond the usual application of scale factors; hence, inaccuracies in the q dependence of one or more of these components of the model could contribute to the remaining systematic errors.

C. Mass independence of the empirical effective interaction

The consistency obtained in Sec. IV A between interactions fitted to inelastic scattering from ^{16}O and ^{40}Ca, either independently or simultaneously, supports the hypothesis that medium depend solely upon local density and are independent of target or state. The consistency obtained in Sec. IV B between interactions fitted to elastic and inelastic scattering, either independently or simultaneously, supports the accuracy of the rearrangement factor relating elastic and inelastic effective interactions. It is also of interest to test the effective interaction for heavier nuclei, such as ^{208}Pb, which should represent a better approximation to infinite nuclear matter. However, the neutron excess presents several complications. First, in the absence of reliable independent measurements of neutron transition densities for nuclei with $N > Z$, fits of the empirical effective interaction to inelastic scattering data must necessarily be restricted to self-conjugate targets. In fact, we have demonstrated that once the effective interaction has been calibrated using data for self-conjugate targets, neutron transition densities for other targets can be measured with proton inelastic scattering [37–39]; of course, it is not possible to fit both the interaction and the structure to the same set of data. Second, medium modifications to the effective in-teraction may depend upon the neutron excess, but no theoretical calculations of the effective interaction for asymmetric nuclear matter are available for energies near 300 MeV. Therefore, rather than attempt to fit the interaction to data for nuclei more massive than calcium, we simply compare data and calculations for elastic scattering that use the present model of the empirical interaction and the best available models of the ground-state density.

Calculations for ^{16}O and ^{208}Pb based on EI-4, the interaction fitted to both elastic and inelastic scattering from ^{40}Ca, are compared in Fig. 11 with calculations based on the FL t matrix and the LR interaction. For ^{16}O we unfold the proton form factor from the charge density of Ref. [40] and assume that $\rho_n = \rho_p$. For ^{208}Pb we use the densities of Ref. [41] constructed by adding a theoretical calculation [42] (DDHFB) of $\rho_n - \rho_p$ to the ρ_p deduced from electron scattering. The cross section and analyzing power for ^{16}O(p,p') at 318 MeV are from Ref. [4]. Cross-section data for ^{208}Pb(p,p') at 318 MeV from Ref. [43] are shown as open circles. Unfortunately, no A_y or SRF data for ^{208}Pb are available at this same energy. The closest available data for A_y are at 300 MeV and for SRF are at 290 MeV, taken from Refs. [44] and [45], respectively. The 300-MeV cross-section data are also
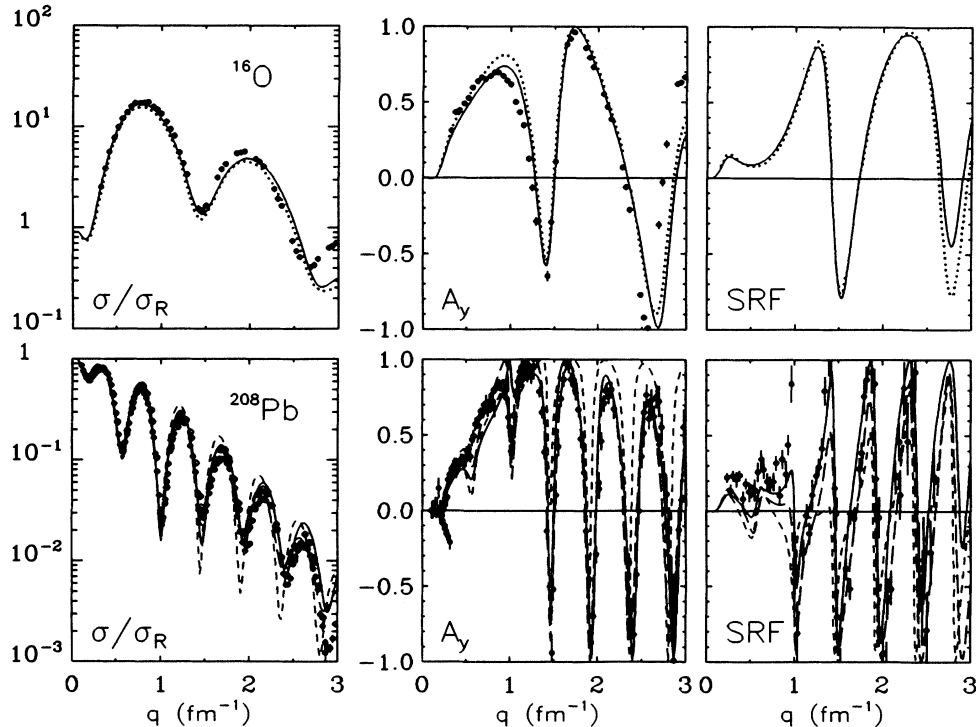

FIG. 11. Calculations for elastic scattering of 318 MeV protons based upon the FL, LR, and EI-4 interactions are shown as short-dashed, long-dashed, and solid curves, respectively. For ^{16}O a calculation based upon the EI-4e interaction fitted to elastic scattering from ^{40}Ca alone is shown by dotted curves. The 318-MeV data for ^{16}O (top row) are from Ref. [4]. Cross-section data for ^{208}Pb (bottom row) at 318 MeV (Ref. [43]) are shown as open circles and cross section and analyzing power data at 300 MeV are shown as filled circles (Ref. [44]). Data for the spin rotation function (SRF) for 290 MeV (Ref. [45]) are also shown as filled circles. Note that cross-section data are shown as ratios σ/σ_R to the Rutherford cross section σ_R so that detailed comparisons may be made. For lead, in particular, use of this ratio reduces the number of decades spanned by these data from 9 to only 3 and enhances clarity considerably.

shown in Fig. 11 as solid circles.

Excellent agreement is obtained with the data for ^{16}O, but the situation for ^{208}Pb is more complicated. Although it appears that the LR interaction gives the most accurate description of both the cross section and analyzing power data, part of this agreement may be fortuitous. As q increases, the discrepancy between the EI-4 calculation of the cross section and the data for 300 MeV increases; however, the 318-MeV cross-section data are somewhat higher at the diffraction peaks and are closer to the EI-4 cross sections. Furthermore, modest changes of the neutron distribution can account for the remaining discrepancies with the cross-section data. We also find that although EI-4 gives a better description of the SRF data than LR, the LR calculation is more accurate for the analyzing power at low q. Although the sharp structure in A_y near 1 fm^{-1} can be reproduced by fitting an interaction to this data, with a result closer to LR than to EI-4, the reliability of such an analysis is difficult to assess in light of uncertainties in the neutron density.

Calculations based upon EI-3 and electroexcitation transition densities were compared with data for ^{32}S(p,p') at 318 MeV in Ref. [39]. We found that good agreement was obtained for this target whose mass lies between those used to fit the interaction. Therefore, there presently exists no evidence for significant mass dependence in the effective interaction for the range $A = 16-40$ and little indication for appreciable mass dependence for $A > 40$. Nevertheless, both the continuing need to apply scale factors to the free interaction and the energy dependence of the comparison between empirical and theoretical interactions suggest that effects due to the finite size of nuclei do require further theoretical investigation.

D. Comparison with relativistic models

These results may be compared with relativistic models of proton elastic scattering via Schrödinger-equivalent potentials which are constructed to give the same elastic scattering with the Schrödinger equation as did the original potentials in the Dirac equation. We compare the EI-4 optical potential with the theoretical prediction of the IA2 version of the relativistic impulse approximation of Ottenstein *et al.* [19] (long dashes) in Fig. 12. The *no-pairs* limit of the IA2 potential is also shown by dotted curves. The latter neglects coupling to virtual $N\bar{N}$ pairs, thus representing the nonrelativistic impulse approximation for the meson-exchange potential of Ref. [46]. The no-pairs approximation to IA2 is qualitatively similar to calculations based upon the FL t matrix. Coupling to virtual $N\bar{N}$ pairs can be described as a source of density dependence in the effective interaction [47]. The dominant effect may be described as a repulsive contribution to Ret^C that is apparently somewhat stronger than that of the nonrelativistic LR interaction, but which is similar to that of the empirical interaction. The density dependence of the imaginary central component of the IA2 interaction is quite small and the corresponding potential is nearly identical with the empirical result.

The optical potentials predicted by the IA2 model are close to those for the empirical interaction for energies

above 300 MeV. For 200 MeV and below, the IA2 model is not nearly as successful in its calculations of elastic scattering. Murdock and Horowitz [48] have shown that substantial improvement of relativistic elastic scattering calculations can be obtained by applying an *ad hoc* Pauli blocking correction to the imaginary central potential. Nonrelativistic LDA calculations naturally include Pauli blocking and are therefore more successful than the IA2 model for energies near 200 MeV. Nevertheless, we have found that significant improvement over LDA calculations based upon interactions from nuclear matter theory can still be obtained using the empirical effective interaction [49]. The real central optical potential then agrees well with the IA2 model, but the imaginary central potential is damped. Evidently, the repulsive contribution to the IA2 interaction from $N\bar{N}$ pairs agrees with the data for 200 MeV, but Pauli blocking must still be added to the IA2 model to obtain an accurate description of absorption. Even though nuclear matter theory would suggest that Pauli blocking remains important at 300 MeV, the apparent absence or diminution of this effect upon the empirical effective interaction leads to good agreement with the IA2 model already by 300 MeV.

We also compare the EI-4 optical potentials with those of Fit 1 from the Dirac phenomenology (DP-1) of Hama *et al.* [20] (long dashes) in Fig. 12. The empirical potentials exhibit more structure than the DP-1 model, which describes the geometry using simple analytic functions which may not be entirely appropriate for a nucleus as small as calcium. The real central potential from DP-1 is
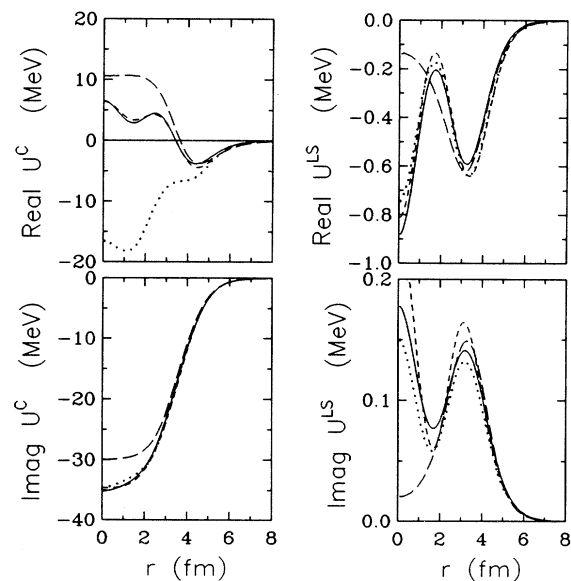

FIG. 12. Relativistic models of the $p + ^{40}$Ca optical potential near 300 MeV are compared with potentials from the EI-4 interaction. The no-pairs limit of the IA2 is illustrated by dotted lines, while full IA2 potentials are shown as short-dashed lines. The latter are quite close to the potentials based upon the empirical effective interaction (solid lines). The potentials from Dirac phenomenology, version DP-1, are shown as long-dashed lines.

similar to the EI-3 potential shown in Fig. 6, except for the oscillation near 2 fm, but is substantially stronger than EI-4 in the interior. Similarly, the spin-orbit potentials are similar near the surface but the DP-1 model is not capable of reproducing the interior oscillation. Perhaps the most significant difference is that the DP-1 imaginary central potential is about 15% smaller than either the EI or the IA-2 results. Nevertheless, the DP-1 imaginary central potential remains nearly 25% stronger than the prediction of the LR model (Fig. 6), supporting our conclusion that the damping effect predicted by that model is not present for energies above 300 MeV. Very similar comparisons between Dirac phenomenology and potentials based upon either the empirical or LR interactions were made at 500 MeV also [5].

We believe that it would be worth investigating whether an alternative fit can be found within the framework of Dirac phenomenology with characteristics closer to the present results, even if χ^2 is not quite as good. The good qualitative agreement obtained between the empirical effective interaction and both relativistic and nonrelativistic models of medium modifications suggests that the very strong repulsion required to reproduce the DP-1 real central potential in the interior is unlikely to properly represent the first-order optical potential for nuclear matter. It is more likely that reduction of ReU^C can be compensated by enhancement of ImU^C with little effect upon the quality of the Dirac fit to the data.

Elastic scattering calculations for ^{40}Ca based upon these potentials from relativistic models are compared with the data and with our EI-4 results in Fig. 13. Dirac phenomenology provides an excellent description of the data even though these data were not included in the analysis of Hama et al. [20]. The IA2 calculations are less successful: even though the pair contributions improve both the cross section and the analyzing power, the IA2 calculations remain significantly above the cross-section data for large momentum transfer. Given the close similarity between the IA2 and EI-4 central potentials, this level of disagreement between scattering calcu-

lations appears surprising. The difficulty may be related to the fact that the IA2 real central and spin-orbit potentials are slightly too strong for large radii, perhaps reflecting an inaccuracy in the model of the free nucleon-nucleon interaction. Also note that we are using IA2 potentials calculated for 300 MeV, the nearest energy for which they are available. Finally, the IA2 calculations employ densities calculated by Horowitz and Serot [50] in the Dirac-Hartree approximation which may contribute to the differences observed at large momentum transfer. Therefore, the qualitative agreement between the IA2 and EI-4 potentials themselves is probably more significant than the disagreement between scattering calculations, which appear to amplify small differences.

V. CONCLUSIONS

We have measured elastic and inelastic scattering of 318 MeV protons from ^{40}Ca and have analyzed the cross section and analyzing power data for normal-parity states using an empirical model of the density dependence of the effective interaction originally based upon nonrelativistic theories of nuclear matter. We find that the effective interaction for 318 MeV protons depends strongly upon local density, but is nearly independent of nucleus or final state. Fits to data for ^{16}O and ^{40}Ca, either independently or simultaneously, yield virtually identical interactions. In fact, the interaction fitted to inelastic scattering from ^{16}O fits both elastic and inelastic scattering from ^{40}Ca equally as well as does a fit to that data itself. The essential characteristics of the empirical effective interaction are independent of ambiguities in the free interaction or details of the parametrization and fitting procedures. Therefore, the hypothesis that medium modifications of the effective interaction depend primarily upon the density in the interaction region and not upon details of nuclear structure is confirmed by our results.

The empirical effective interaction differs from the results of recent nonrelativistic theories in two important
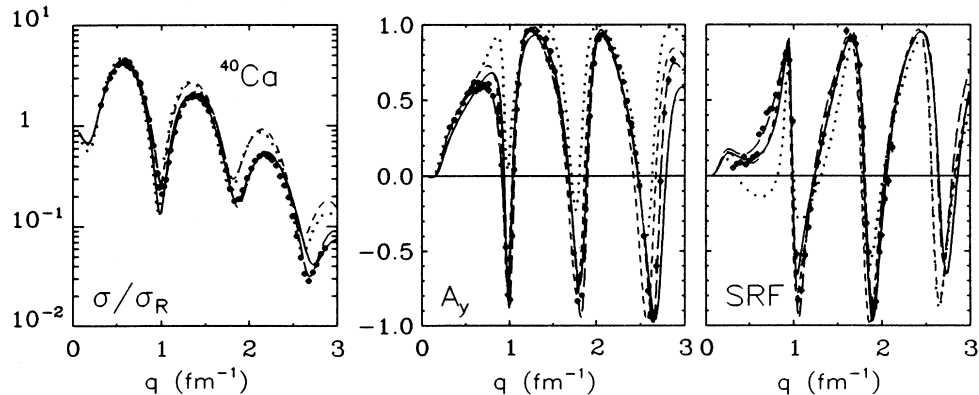

FIG. 13. Elastic scattering calculations are compared with the data for $p + {}^{40}$Ca at 318 MeV. The no-pairs limit of IA2 is indicated by dotted lines, full IA2 calculations are shown as short-dashed lines, and the prediction of the global Dirac phenomenology DP-1 is illustrated by long-dashed lines. We also include the EI-4 calculation, as solid lines, for comparison.

respects. First, the repulsive contribution to the real central interaction appears to be about twice as strong as predicted by nonrelativistic theories. Second, Pauli blocking of absorption appears to be obscured by a new absorptive mechanism which is strong enough to cancel the Pauli effect and to produce a small enhancement of absorption. Both of these effects are also present and are stronger for the empirical effective interaction fitted to ^{16}O and ^{40}Ca$(\vec{p},\vec{p}')$ data for 500-MeV protons.

Optical potentials calculated from the empirical effective interaction were compared with the Schrödinger-equivalent potentials from the relativistic IA2 model and from Dirac phenomenology. The density dependence arising in the IA2 model from coupling to virtual $N\overline{N}$ pairs is very similar to our nonrelativistic fit to inelastic scattering data. These potentials are also similar to Dirac phenomenology, but have somewhat more structure than can be accommodated by simple analytic functions. As also found at 500 MeV, the empirical interaction and the IA2 model produce somewhat stronger imaginary and weaker real central potentials than Dirac phenomenology.

The ability of an interaction fitted to inelastic scattering by ^{16}O to reproduce both elastic and inelastic scattering from ^{40}Ca is truly remarkable. We find that above 300 MeV the optical potentials from the empirical interaction are closer to those of relativistic models than to those from nonrelativistic theories of the effective interaction, but that below 200 MeV the nonrelativistic nuclear matter models are more successful. Therefore, it would appear profitable to merge the approaches by inclusion of Pauli blocking and self-energy corrections in a relativistic theory of the effective interaction in nuclear matter. For a more quantitative understanding of proton scattering, it will be necessary to perform further study of finite-nucleus corrections to the LDA and of full-folding corrections [51], both of which are implicitly subsumed by the empirical interaction. The success of the empirical effective interaction suggests that a parametrization of this type should remain a useful representation and vehicle for comparison of models of proton-nucleus scattering.

*Present address: Department of Physics, American University, Washington, D.C. 20016.
†Present address: NINDS/NIH, Bethesda, MD 20892.
‡Present address: NASA-Goddard Space Flight Center, Greenbelt, MD 20771.

[1] H. V. von Geramb, in *The Interaction Between Medium Energy Nucleons in Nuclei (Indiana Cyclotron Facility, Bloomington, Indiana)*, Proceedings of the Workshop on the Interactions Between Medium Energy Nucleons in Nuclei, edited by Hans-Otto Meyer, AIP Conf. Proc. No. 97 (AIP, New York, 1982), p. 44; L. Rikus, K. Nakano, and H. V. von Geramb, Nucl. Phys. A414, 413 (1984).

[2] K. Nakayama and W. G. Love, Phys. Rev. C 38, 51 (1988).

[3] L. Ray, Phys. Rev. C 41, 2816 (1990).

[4] J. J. Kelly, A. E. Feldman, B. S. Flanders, H. Seifert, D. Lopiano, B. Aas, A. Azizi, G. Igo, G. Weston, C. Whitten, M. V. Hynes, J. McClelland, W. Bertozzi, J. M. Finn, C. E. Hyde-Wright, R. W. Lourie, P. E. Ulmer, B. E. Norum, and B. L. Berman, Phys. Rev. C 43, 1272 (1991).

[5] B. S. Flanders, J. J. Kelly, H. Seifert, D. Lopiano, B. Aas, A. Azizi, G. Igo, G. Weston, C. Whitten, A. Wong, M. V. Hynes, J. McClelland, W. Bertozzi, J. M. Finn, C. E. Hyde-Wright, R. W. Lourie, B. E. Norum, P. Ulmer, and B. L. Berman, Phys. Rev. C 43, 2103 (1991).

[6] J. Hüfner and C. Mahaux, Ann. Phys. (N.Y.) 73, 535 (1972).

[7] F. A. Brieva and J. R. Rook, Nucl. Phys. A291, 299 (1977); A291, 317 (1977); A297, 206 (1978); A307, 493 (1978); H. V. von Geramb, F. A. Brieva, and J. R. Rook, in *Microscopic Optical Potentials*, edited by H. V. von Geramb (Springer-Verlag, Berlin, 1979), p. 104.

[8] J. Kelly, W. Bertozzi, T. N. Buti, F. W. Hersman, C. Hyde, M. V. Hynes, B. Norum, F. N. Rad, A. D. Bacher, G. T. Emery, C. C. Foster, W. P. Jones, D. W. Miller, B. L. Berman, W. G. Love, and F. Petrovich, Phys. Rev. Lett. 45, 2012 (1980).

[9] J. J. Kelly, W. Bertozzi, T. N. Buti, J. M. Finn, F. W. Hersman, C. E. Hyde-Wright, M. V. Hynes, M. A. Kovash, B. Murdock, B. E. Norum, B. Pugh, F. N. Rad, A. D. Bacher, G. T. Emery, C. C. Foster, W. P. Jones, D. W. Miller, B. L. Berman, W. G. Love, J. A. Carr, and F. Petrovich, Phys. Rev. C 39, 1222 (1989).

[10] M. Lacombe, B. Loiseau, J. M. Richard, R. Vinh Mau, J. Cote, P. Pires, and R. de Tourreil, Phys. Rev. C 21, 861 (1980).

[11] P. J. Siemens, Nucl. Phys. A141, 225 (1970).

[12] R. Machleidt, K. Holinde, and Ch. Elster, Phys. Rep. 149, 1 (1987).

[13] E. L. Lomon and H. Feshbach, Ann. Phys. (N.Y.) 48, 94 (1968); E. L. Lomon, Phys. Rev. D 26, 576 (1982).

[14] K. M. Watson, Phys. Rev. 89, 575 (1953).

[15] J. J. Kelly, Phys. Rev. C 39, 2120 (1989).

[16] J. J. Kelly, J. M. Finn, W. Bertozzi, T. N. Buti, F. W. Hersman, C. Hyde-Wright, M. V. Hynes, M. A. Kovash, B. Murdock, P. Ulmer, A. D. Bacher, G. T. Emery, C. C. Foster, W. P. Jones, D. W. Miller, and B. L. Berman, Phys. Rev. C 41, 2504 (1990); Q. Chen, J. J. Kelly, P. P. Singh, M. C. Radhakrishna, W. P. Jones, and H. Nann, *ibid.* 41, 2514 (1990).

[17] E. Clementel and C. Villi, Nuovo Cimento 2, 176 (1955).

[18] T. Cheon, K. Takayanagi, and K. Yazaki, Nucl. Phys. A437, 301 (1985); A445, 227 (1985); T. Cheon and K. Takayangi, *ibid.* A445, 653 (1986).

[19] N. Ottenstein, S. J. Wallace, and J. A. Tjon, Phys. Rev. C

38, 2272 (1988); **38**, 2289 (1988).

[20] S. Hama, B. C. Clark, E. D. Cooper, H. S. Sherif, and R. L. Mercer, Phys. Rev. C **41**, 2737 (1990).

[21] L. G. Atencio, J. A. Amann, R. L. Boudrie, and C. L. Morris, Nucl. Instrum. Methods **187**, 381 (1981).

[22] M. W. McNaughton, Los Alamos Scientific Laboratory Report LA-8307, 1980 (unpublished).

[23] R. A. Arndt, program SAID (unpublished); R. A. Arndt, L. D. Roper, R. A. Bryan, R. B. Clark, B. J. VerWest, and P. Signell, Phys. Rev. D **28**, 97 (1983).

[24] A. E. Feldman, University of Maryland, Ph.D. thesis (1991).

[25] J. J. Kelly, computer program ALLFIT (unpublished).

[26] P. M. Endt and C. van der Leun, Nucl. Phys. **A310**, 1 (1978).

[27] See AIP document No. PAPS PRC-44-2602-39 for 39 pages containing a complete tabulation of the data described in this paper. Order by PAPS number and journal reference from American Institute of Physics, Physics Auxiliary Publication Service, 335 E. 45th Street, New York, NY 10017. The price is $1.50 for each microfiche or $6.35 for photocopies. Air mail additional. Make checks payable to the American Institute of Physics.

[28] H. deVries, C. W. deJager, and C. deVries, At. Data Nucl. Data Tables **36**, 495 (1987).

[29] R. A. Miskimen, Ph.D. thesis, Massachusetts Institute of Technology, 1983.

[30] P. Harihar, K. K. Seth, D. Barlow, S. Iverson, M. Kaletka, H. Nann, A. Saha, C. F. Williamson, J. W. Wong, M. Deady, and W. J. Gerace, Phys. Rev. Lett. **53**, 152 (1984).

[31] A. K. Kerman, H. McManus, and R. M. Thaler, Ann. Phys. (N.Y.) **8**, 551 (1959).

[32] M. A. Franey and W. G. Love, Phys. Rev. C **31**, 488 (1985).

[33] G. G. Ohlsen, Rep. Prog. Phys. **35**, 717 (1972).

[34] J. J. Kelly, computer program LEA (unpublished).

[35] P. R. Bevington, *Data Reduction and Error Analysis for the Physical Sciences* (McGraw-Hill, New York, 1969).

[36] E. Bleszynski, B. Aas, D. Adams, M. Bleszynski, G. J. Igo, T. Jaroszewicz, A. Ling, D. Lopiano, F. Sperisen, M. G. Moshi, C. A. Whitten, K. Jones, and J. B. McCelland, Phys. Rev. C **37**, 1527 (1988).

[37] J. J. Kelly, Phys. Rev C **37**, 520 (1988).

[38] J. J. Kelly, Q. Chen, P. P. Singh, M. C. Radhakrishna, W. P. Jones, and H. Nann, Phys. Rev. C **41**, 2525 (1990).

[39] M. A. Khandaker, J. J. Kelly, P. Boberg, A. E. Feldman, B. S. Flanders, S. Hyman, H. Seifert, P. Karen, B. E. Norum, P. Welch, S. Nanda, and A. Saha, Phys. Rev. C **44**, 1978 (1991).

[40] The ^{16}O density due to G. Lahm (Ph.D. thesis, University of Mainz, 1986) may be found tabulated in Ref. [28].

[41] L. Ray and G. W. Hoffman, Phys. Rev. C **31**, 538 (1985).

[42] J. Decharge and D. Gogny, Phys. Rev. C **21**, 1568 (1980); J. Decharge, M. Girod, D. Gogny, and B. Grammaticos, Nucl. Phys. **A538**, 203c (1981).

[43] N. M. Hintz, D. Cook, M. Gazzaly, M. A. Franey, M. L. Barlett, G. W. Hoffman, R. Fergerson, J. McGill, J. B. McClelland, and K. W. Jones, Phys. Rev. C **37**, 692 (1988).

[44] D. A. Hutcheon, W. C. Olsen, H. S. Sherif, R. Dymarz, J. M. Cameron, J. Johansson, P. Kitching, R. P. Liljestrand, W. J. McDonald, C. A. Miller, G. C. Neilson, D. M. Sheppard, D. K. McDaniels, J. R. Tinsley, P. Schwandt, L. W. Swenson, and C. E. Stronach, Nucl. Phys. **A483**, 429 (1988).

[45] O. Häusser, K. Hicks, C. W. Glover, R. Abegg, A. Celler, C. Günther, R. L. Helmer, R. Henderson, D. J. Horen, C. J. Horowitz, K. P. Jackson, J. Lisantti, D. K. McDaniels, C. A. Miller, R. Sawafta, and L. W. Swenson, Phys. Lett. B **184**, 316 (1987).

[46] E. E. van Faassen and J. A. Tjon, Phys. Rev. C **28**, 2354 (1983); **30**, 285 (1984).

[47] M. V. Hynes, A. Picklesimer, P. C. Tandy, and R. M. Thaler, Phys. Rev. Lett. **52**, 978 (1984).

[48] D. P. Murdock and C. J. Horowitz, Phys. Rev. C **35**, 1442 (1987).

[49] H. Seifert, University of Maryland, Ph.D. thesis, 1990.

[50] C. J. Horowitz and B. D. Serot, Nucl. Phys. **A368**, 503 (1981).

[51] H. F. Arellano, F. A. Brieva, and W. G. Love, Phys. Rev. Lett. **63**, 605 (1989); Phys. Rev. C **41**, 2188 (1990).